# Toward Sub-gram Helicopters: Designing a Miniaturized Flybar for Passive Stability

Kyle Johnson[1†*], Vicente Arroyos[1†], Raul Villanueva[2†], Adriana Schulz[1], Sawyer Fuller[3], Vikram Iyer[1*]
[1] Paul Allen School of Computer Science and Engineering, University of Washington
[2] Department of Electrical and Computer Engineering, University of Washington
[3] Department of Mechanical Engineering, University of Washington
[†] Equal and primary contribution first authors
[*]Corresponding authors

***Abstract*— Sub-gram flying robots have transformative potential in applications from search and rescue to precision agriculture to environmental monitoring. However, a key gap in achieving autonomous flight for these applications is the low lift to weight ratio of flapping wing and quadrotor designs around 1 g or less. To close this gap, we propose a helictoper-style design that minimizes size and weight by leveraging the high lift, reliability, and low-voltage of sub-gram motors. We take an important step to enable this goal by designing a light-weight, micfrofabricated flybar mechanism to passively stabilize such a robot. Our 48 mg flybar is folded from a flat carbon fiber laminate into a 3D mechanism that couples tilting of the flybar to a change in the angle of attack of the rotors. Our design uses flexure joints instead of ball-in-socket joints common in larger flybars. To expedite the design exploration and optimization of a microfabricated flat-folded flybar, we develop a novel user-in-the-loop bi-level optimization workflow that combines Bayesian optimization design tools and expert feedback. We develop four template designs and use this method to achieve a peak damping ratio of 0.528, an 18.9x improvement from our initial design. Compared to a flybar-less rotor with a near 0 damping ratio, our flybar-rotor mechanism maintains a stable roll and pitch with relative deviations <1°. Our results show that, if combined with a counter-torque mechanism such as a tail rotor, our miniaturized flybar could mechanically provide attitude stability for a sub-gram helicopter.**

## I. Introduction

Sub-gram aerial robots have transformative potential for applications including search and rescue missions, gas leak detection, wireless networking, 3D mapping, and environment monitoring. Their advantages originate from low materials cost, with potential for greater deployment numbers as coordinated swarms with a myriad of different sensor attachments. Their small size also enables navigation in confined spaces indoors or at disaster sites, gathering sensory data from precise locations in 3D space, and operation around humans without impact hazard. Additionally, recent work has shown scaling down in mass is favorable for energy harvesting, and identifies an optimal mass of 1 g or lower to enable extended airtime or battery-free operation [1].

Despite significant interest over two decades, state of the art robots weighing less than ∼1 g have not achieved this goal due to the challenges of miniaturizing actuators, batteries, and sensing and control systems [2, 3, 13–15]. Fig 1A shows a survey of recent flapping-wing and four-rotor ("quadrotor") designs and their lift to weight ratios, including total mass of onboard batteries or power harvesting. We observe that a key performance gap for small vehicles is a low lift-to-weight ratio [8].

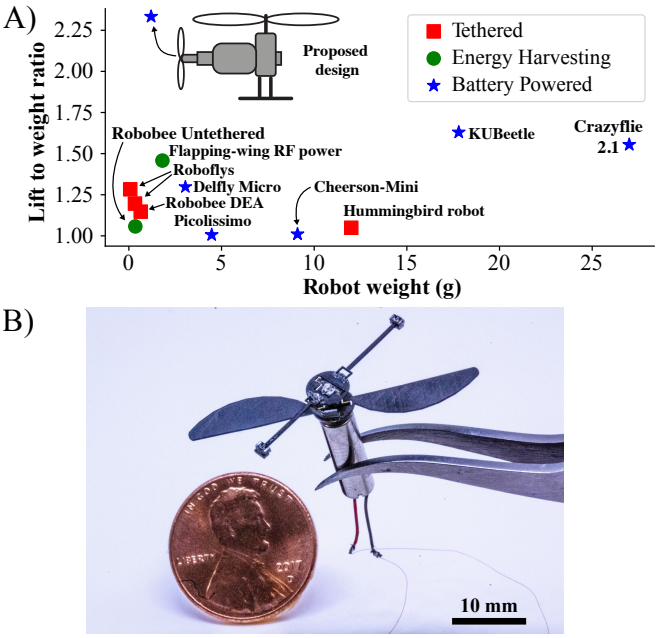


Fig. 1. A) Plot of lift to weight ratio, including mass of battery and power harvesting payload, for small aerial robots: Roboflys [2, 3], Robobee DEA [4], Robobee Untethered [5], Piccolissimo [6], Cheerson-Mini [7], Crazyflie 2.1 [8], Flapping-wing RF power [9], KUBeetle [10], Hummingbird robot [11], and DelFly Micro [12]. B) Flybar-rotor mechanism attached to a motor. Flybar tilting mechanically changes the rotor angle of attack.

We propose the design of a sub-gram helicopter, shown in Fig 1A. Our key observation is that a single rotor (2-3 cm) used in a small quadrotor [8] can weigh less than 1 g, and can produce a substantial lift force (2.8 g) [16]. This lift is more than sufficient to carry a sub-gram battery and a ∼200 mg avionics system onboard [3]. Using a single, larger-thrust motor instead of 4 smaller motors reduces the negative efficiency and power density penalty associated with reducing scale in small electromagnetic motors. Four motors, each at 1/4 the power, either dissipate significantly

*This research was partially supported by the National Science Foundation (award number FRR-2054850).

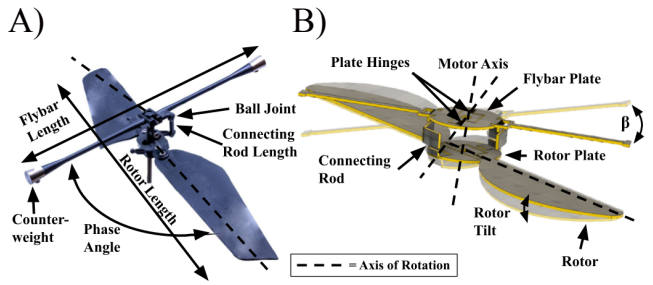


Fig. 2. A) Labeled diagram of a model helicopter's flybar indicating parameters used in our design workflow. B) Labeled CAD diagram of foldable flybar design indicating design elements and rotation axis. Tilting of the flybar induces a tilt in the rotor blades through the connecting rods.

more heat per watt produced, or suffer from much lower power density measured in watts per kg [17]. To stabilize a sub-gram helicopter without additional motors, we propose a passive stabilization mechanism to enable single-motor flight. Toward this goal, we design and optimize a first-of-its kind foldable flybar stabilization mechanism measuring 2-3 cm, shown in Fig 1B and Fig 2.

Traditional quadrotors become very inefficient near the 1 g scale [7], exhibiting low controllability and payload capacity. As a result, most near gram designs rely on non-rotor lift generation, primarily using piezoelectric cantilever actuators to drive insect-like flapping wings. Piezo actuators have high power density and the ability to control each wing independently, making it possible to perform controlled hover [18]. However, they generate low lift ($\sim$100-200 mg), which severely restricts the robot's payload capacity [19]. Piezos are also driven near the limit of their performance to achieve sufficient lift, requiring $>$200 V [5, 19]. Adding a bespoke and heavy boost converter onboard further reduces the end-to-end efficiency and lift to weight ratio.

Recent works have explored devices using multiple or larger actuators to increase lift [5, 9, 20], but they cannot yet carry a battery capable of powering their actuators. Untethered designs rely on harvested energy, but only from high power external sources that limit the device's mobility [5, 9].

We observe that actuation and control mechanisms account for most of the power and mass in small aerial robots. Our miniaturization strategy aims to leverage the high thrust of electric motors, rather than modifying the actuators, to design a helicopter which minimizes the number of actuators required. Combining a 0.55 g motor with a lightweight avionics system [3] and tail actuator could enable a design with total mass of $\sim$1 g, as shown in Fig 1.

Designing a sub-gram helicopter presents unique challenges. For example, the main rotor produces a counter torque on the body with an asymmetric lift force [21]. During forward motion, a difference in relative airflow on each half of the rotor disk produces greater lift on the advancing rotor blade, and lower lift on the retreating blade. In the case of counterclockwise rotation, this will result in a net roll to the left. Conventional helicopters have long blades with low stiffness, causing aero-elastic flapping that feathers this effect [22]. However, blade stiffness is inversely proportional to rotor length $\ell^3$, resulting in a negligible flexing of the rotor during flight at the 2-3 cm scale.

Recent works have explored single rotor stabilization by rotating the robot body [6, 23]. These designs require smooth landing and lift off surfaces, raising serious challenges in aiming a sensor like a camera or adding other payloads.

Alternatively, larger robots like helicopters have achieved passive stability using a flybar [22, 24, 25]. Flybars, freely hinged weighted paddles attached to the main rotor of small helicopters, help stabilize attitude dynamics. In the case of hovering, if a wind gust or other disturbance rotates the aircraft out of equilibrium, the flybar will continue spinning in the same inertial plane. This angle change with respect to the main rotor pushes the aircraft back to equilibrium. Researchers of flapping wing robots favor passive wing joints over actively controlling the wing's angle of attack [13, 19]; similarily, an effective flybar at this scale would be a key enabling technology for miniaturized helicopters.

Designing a flybar at this scale has multiple challenges. First, it requires the design and fabrication of joints that allow the flybar to bend with respect to the robot body, and couple that to changes in the rotor's angle of attack. Large helicopter flybars use ball and socket joints which permit arbitrary rotation. At small scale, ball joints are subject to high coulomb friction due to the increase in friction relative to inertial forces as scale reduces. For an aircraft with length scale $\ell$, the surface area of components scales down at a rate of $\ell^2$, while inertial and gravitational forces scale down at a rate of $\ell^3$. A biology-inspired alternative is to replace such joints, which do not have to perform complete revolutions, with flexure (hinge) joints not subject to coulomb friction.

Second, the design must be optimized for operation at small scale. While prior studies have modeled and optimized flybar designs orders of magnitude larger [22], these insights may not translate because of scale-dependent effects that include friction, aerodynamic, and inertial forces. Moreover, fabrication constraints may preclude the use of conventional design methodologies at the 2-3 cm scale. This makes it challenging to effectively explore the design space due to the time and effort required to fabricate new prototypes.

Third, while it may be possible to fabricate a small flybar with the appropriate range of motion, it requires a complicated analysis to determine whether the aforementioned differences associated with small scale will allow for a sufficient stabilization effect. If improperly designed an additional spin in phase with the main rotor could produce positive feedback that further destabilizes the aircraft. An effective design must contribute damping to the system, but characterizing this also requires an effective evaluation apparatus to perform consistent, repeatable experiments.
The following contributions address these challenges:

- **Foldable flybar design.** We develop a first-of-its-kind foldable flybar mechanism. The entire design can be folded from a flat carbon fiber laminate into a 3D mechanism 24 mm in length and weighing 48 mg (without counterweights). Our design successfully replicates the motion of dual spherical ball joints in traditional flybars to couple tilt to rotor blade angle of attack with a compact 2 mm linkage.

• **Computational design for miniaturization.** We demonstrate a novel workflow that combines computational design software with expert input to effectively navigate the mechanism's 2-3 cm design space. Our key insight is that while computational design optimization is typically limited to well-defined search spaces where physical simulation can be applied, we use it when neither of these assumptions hold as feedback to the expert designers. Specifically, we use Bayesian optimization and show how the output of the optimizer can help users understand whether they are exploring the correct part of the design space. By combining computation and expert knowledge we expedite design exploration for improving flybar performance.

• **Functional flybar measuring 2-3 cm.** We demonstrate the first functional flybar mechanism at the 2-3 cm scale achieving a damping ratio of $\zeta = 0.528$. Compared to a flybar-less motor, which oscillates chaotically ($\zeta = 0.007$), our flybar maintains a stable orientation in roll and pitch with relative deviations of less than 1°.

In the remainder of the paper, we will first describe the flybar dynamics and its operation, followed by a detailed description of our final foldable design and fabrication process. We will then describe our iterative design workflow for optimizing the flybar's damping ratio, followed by our evaluation results. We conclude with discussing future works, specifically with how a sub-gram helicopter measuring 2-3 cm could leverage this mechanism to achieve autonomy.

## II. Designing a Foldable Flybar

We describe the principles of operation for a flybar and a description of our folding design and fabrication methods.

### A. Flybar dynamics

A flybar or stabilizer bar, is a passive damping mechanism used to help stabilize helicopters through gyroscopic forces. A key difference in small helicopters is increased stiffness due to short rotor length which prevents the blade flexing that helps stabilize larger aircraft. Additional actuators for actively controlling the rotor's angle of attack become infeasible at the 2-3 cm scale due to size and weight constraints.

A flybar consists of a two-sided weighted paddle or airfoil that rotates in tandem with the main rotor of a helicopter, connected so that the blades of the main rotor vary their angle of attack ("feathering") on a phase-dependent basis as the rotor moves around the drive axle. This feathering results in applied torque to the helicopter body as the rotor spins. Fig 2 shows the main components and geometry of a flybar. This includes the counterweights at the tips of the flybar which increase its angular momentum, the hinged rotor plate which connects the mechanism to the motor axis, and the connecting rod which links the flybar to the main rotor. The hinges in the connecting rod and rotor plate allow the flybar to spin in a plane rotated by an angle $\beta$ about an axis perpendicular to the axis of rotation of the rotor's drive shaft and pivot with respect to the body.

Pivoting with respect to the body is key to stabilizing. When the aircraft is disturbed by wind, gyroscopic forces keep the flybar rotating in the same plane (0°) as the inclination angle of the helicopter body changes. For example, if the helicopter rolls right, the linkage between the flybar and the main rotor causes the main rotor disk to tilt changing the blade pitch. The resulting lift change pushes the aircraft back towards 0°.

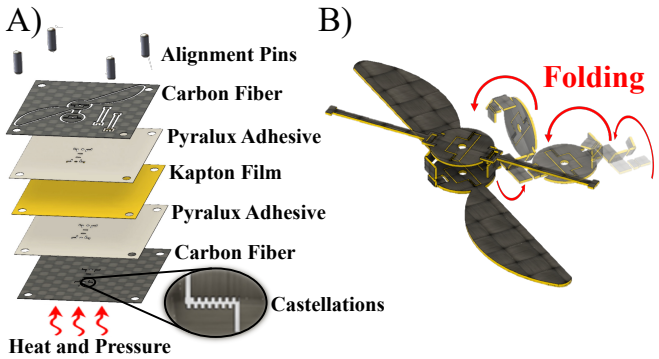


Fig. 3. A) Pin aligned laminate showing the 5 layer stack and castellated hinge joints with micrometer-size features. B) Arrows indicate the folds used to assemble the flat laminate Final Template design into a 3D flybar.

If the angle between the flybar's axis of rotation and the main rotor's feathering degree of freedom's axis of rotation is between 0 and 180°, then the feathering action re-rights the helicopter, counteracting its otherwise inherent instability. A simplified model of the net torque acting on the helicopter body due to the action of the flybar is given by [22]

$$\tau = -\lambda_1 \Omega^2 \beta - \lambda_2 \Omega \dot{\beta}, \quad (1)$$

$\tau$ is the torque acting on the body arising from the feathering action induced by the flybar. This equation holds for the pitch and roll axis. $\Omega$ is the angular velocity of the main rotor axle (assumed to be constant), $\dot{\beta}$ is the angular velocity of the helicopter body (about that body-attached axis), and $\lambda_1$ and $\lambda_2$ are constants that depend on the geometry of the system, such as pullrod lengths, rotor length and blade inclination angles, and the aerodynamic lift coefficient of the main rotor.

This assumes the flybar is rotating in a level plane (e.g. hovering), and the vehicle has inclined by an angle $\beta$ (flybar tilt). Equation 1 shows that the flybar acts both as a damper (with damping coefficient $\lambda_2 \Omega$) and a spring-like angle-dependent restoring torque that depends on $\beta$. Like in small flapping-wing robots, if the damping coefficient is large enough, then the coupled lateral-rotational dynamics of the hovering system can be stabilized [26]. We assume the flybar remains level, but in practice, its angle slowly decays to the plane of the main rotor due to drag and resilience in the linkage mechanism, with a time constant much slower than the attitude dynamics of aircarft body so this can be neglected. Modeling of the dynamics can be found in [22].

To maximize its effect on the main rotor blade, the flybar is attached at an angle (at 90° in Fig 2A and at ≈45° in Fig 2B). This angle compensates for the effect of gyroscopic precession, which causes angular lag in the output. In large helicopters, this angle is typically 90°. For example, a downward pitch at the front of the helicopter will manifest as a rightward change in roll. In order for the flybar to have the desired effect on the rotor blades, it is

therefore placed at an angle to allow for maximum effect on the rotors accounting for precession. In small helicopters with lightweight rotors, low body mass, and or low head speed, an acute angle is more effective [27].

### B. Folding mechanism design

We seek to replicate the motion of traditional flybars using flat folding structures to reduce coulomb friction in millimeter scale spherical joints and enable rapid fabrication with lightweight materials. This is challenging due to complex required rotation. First, the flybar must be coupled to the motor axle to spin, but must also freely pivot with respect to this axis to achieve its stabilizing functionality. Second, the flybar must be coupled to the main rotor to change the blade pitch. A rigid four bar linkage would not produce a small twisting motion required for acute phase angles. Larger scale flybars use ball joints at *both* the attachment to the flybar and rotor. Prior folded spherical five bars are larger, do not fit the geometry required, and only have one spherical joint [28].

To design this motion we create hinges on the rotor hubs for the flybar and main rotor as shown in Fig 2B. The structure consists of hinges on either side of the motor axle and must be aligned with the center of the axle to produce symmetric motion. The T-shaped structure is designed to be wide enough to accommodate the axle and has a channel cut around it that allows it bend freely out of plane enabling the flybar to maintain its orientation as the aircraft body tilts.

Next we couple the hinged plates with connecting rods to translate flybar tilt to rotor blade pitch. For phase angles less than 90°, the internal hinges on the flybar plate and rotor plate are no longer parallel meaning the bending motion of the flybar must be translated to be applied to the correct axis of the rotor plate. To address this we design a connecting rod with 3 flexures shown in Fig 2B. The first flexure allows the flybar to tilt and connects to two horizontal pieces of carbon fiber connected by a second flexure. This flexure is glued at a fixed angle, and connects to a third movable flexure which attaches to the main rotor. The combination of these 12 flexures enable the flybar's rotation.

### C. Fabrication process

We manufacture these 3D dynamic structures from a composite laminate of five flat sheets shown in Fig 3. The rigid outer layers are made of 95 µm thick carbon fiber sheets with 4 layers of 23 grams per square meter (GSM) carbon fiber arranged in a 4-ply 0°–45°–315°–0° stack. The center layer consists of a polyimide sheet (7.5 µm or 12.5 µm), which acts as a hinge. We use an acrylic sheet adhesive (FR1500 Pyralux) to bond them together.

We begin by designing the cut patterns in a vector drawing program (Vectorworks). We then use these designs to pattern each layer using a laser micromachining system (LPKF Protolaser U4) as shown in Fig 3. The carbon fiber layers are patterned with cuts to define the edges of the flybar and rotor structure and features such as the teeth of the castellated hinges. Each sheet is cut on a standard 29 mm square with pin alignment holes in the corners. The remaining layers are also cut and then placed in a heat press for 1.5 hrs at 205°C at a pressure of 50 - 60 kgf/cm$^2$. The flybar structure is removed from the square sheet with a release cut. The final structure is folded manually into its 3D shape, and attachment points are secured with cyanoacrylate (CA) glue. This process results in a flexible, lightweight structure (46-54 mg) with a total production time of 2.5-3 hrs per prototype.

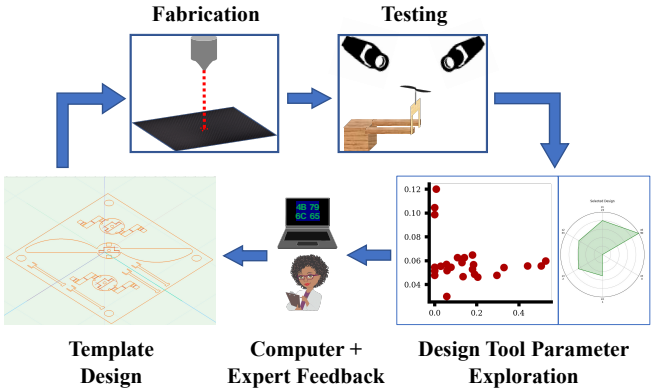


Fig. 4. User-in-the-loop bi-level optimization workflow, combining computational design tools and expert feedback to expedite the exploration of new prototype designs in a changing design space.

## III. Computational Design Optimization

Scaling a flybar, and robotic mechanisms generally, to millimeter scale often results in unexpected design complications which makes defining the design space and optimizing mechanisms challenging. Our design cannot use spherical joints and reducing the length scale by orders of magnitude from traditional designs increases stiffness and may break other large scale model assumptions. We develop a novel workflow leveraging insights from computational design tools and expert user in the loop feedback shown in Fig 4.

### A. Design tools for miniaturization

There are two key considerations in design for miniaturization. First, miniaturization requires different fabrication techniques, which constrains mechanical performance. We must understand what aspects of the behavior must be preserved and how to map them to manufacturing. For example, many insect scale robots are fabricated with flexures instead of revolute joints. The impact of high-level decisions on the design are hard to predict and require iteration.

Second, even once designers understand the design structure, there is still the question of how to tune specific parameters such as dimensions, angles, and material properties for miniaturization. Many mechanisms are well studied and modeled at large scale, but these models may neglect or approximate factors that are important at millimeter scale. For example, small rotor blades do not experience aeroelastic flapping which helps stabilize larger helicopters.

These considerations make design for miniaturization a bi-level optimization problem, characterized by *nested* optimization loops. The outer loop refers to the step of creating a design prototype with a set of exposed parameters that can be optimized, we will call this prototype a *design template*. For each design template, we must then search over the exposed

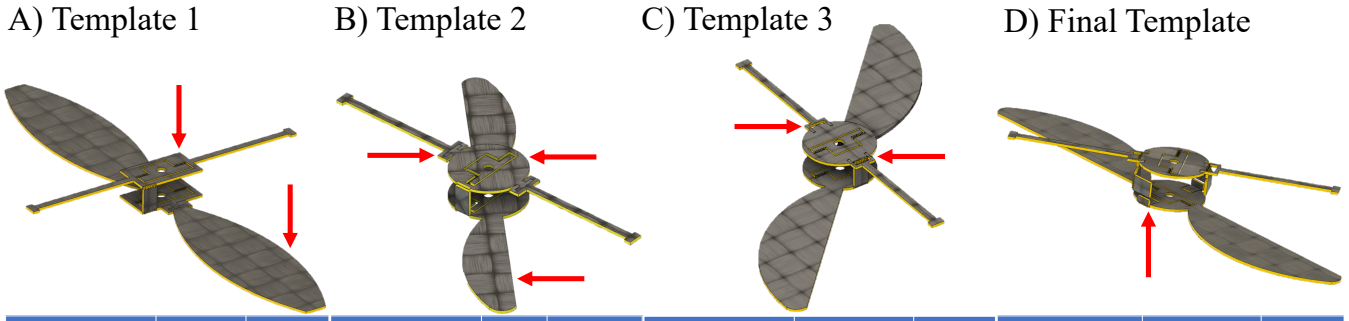


| Parameters | Inputs | Bounds |
|---|---|---|
| 1. Flybar Len. | 22, 22, 22 | 0 - 4 cm |
| 2. Propeller Len. | 46, 46, 44 | 0 - 5 cm |
| 3. Pullrod Len. | 2, 2.5, 2 | 0 - .5 cm |
| 4. Counter Wgt. | .1, .1, .1 | 0 - 5 cm |

| Parameters | Inputs | Bounds |
|---|---|---|
| 1. Flybar Len. | 22, 22 | 0 - 4 cm |
| 2. Propeller Len. | 40, 40 | 0 – 4.5 cm |
| 3. Pullrod Len. | 2, 2 | 0 - .4 cm |
| 4. Counter Wgt. | .1, .1 | 0 - 5 cm |
| 5. Phase Angle | 90, 45 | 45 - 90° |

| Parameters | Inputs | Bounds |
|---|---|---|
| 1. Flybar Len. | 24, 24, 24, 24 | 0 - 3 cm |
| 2. Propeller Len. | 33, 33, 33, 33 | 2 - 4 cm |
| 3. Pullrod Len. | 0, 2, 2, 2 | 0 - .3 cm |
| 4. Counter Wgt. | 0, .1, .1, .1 | 0 – 5 cm |
| 5. Phase Angle | 0, 45, 45, 90 | 0 - 90° |
| 6. # of Pullrods | 0, 1, 2, 2 | 0 - 2 |

| Parameters | Inputs | Bounds |
|---|---|---|
| 1. Pullrod Len. | 3, 2.5, 3, 3 | 0 - .3 cm |
| 2. Counter Wgt. | .1, .1, 8, 12 | 0 - 5 cm |
| 3. Phase Angle | 10, 45, 45, 45 | 0 - 90° |
| 4. # of Pullrods | 2, 2, 2, 2 | 0 - 2 |

Fig. 5. Flybar design templates: A) Template 1. The unique features of this design is the rectangular flybar and propeller plates, as well as the lack of a leading edge on the propellers. B) Template 2. The unique features of the design are the rounding of the flybar and propeller plates, leading edges on the propellers, and manual puzzle piece like attachments for the flybars. C) Template 3. The unique features of the design were the changed axis of rotation for the connecting rod between and a manual attachment for the flybar that fit into cutouts of the top layer of the laminate. D) Final Template. The unique feature of the design is the altered connecting pullrod to allow for 45 degree alpha angles between the two plates that properly feathers the rotor.

template parameters to find the best performing configuration, this is the inner loop of the nested optimization.

Bi-level optimization problems are notoriously expensive to solve, given their nested structure. In this case, we have the added challenge of performance evaluation. Existing large scale models for physical simulation often do not account for scaling effects that occur at low mass or small dimensions. For example, empirical observations have shown the angular lag in control outputs to be less than 90° in small designs [27] but is not well studied. Because of this we must physically test models to evaluate performance. Since fabrication-in-the loop evaluation is expensive and time-consuming, taking ∼3 hours to fabricate, we need to minimize the number of tests.

### *B. User-in-the-loop Bi-level Optimization Workflow*

We propose a workflow for designing miniaturized mechanisms to address the challenges of bi-level optimization with fabrication-in-the-loop evaluation. Our goal is to use computational design optimization in conjunction with expert input to efficiently explore the space.

Despite recent advances in design optimization [29–31], these typically assume a well-defined design space to search. As a result, they can be applied for template parameter optimization (inner loop) but are less useful for template exploration (outer loop), where the space is not easily represented. In addition, optimization requires evaluating a large sample size, which is challenging in our domain.

To address these challenges, our design workflow is driven by two design decisions. First, we propose to use Bayesian optimization to explore the parameter space of a given template. Bayesian optimization is effective when design evaluation is expensive because it suggests a small number of samples [32]. However, Bayesian optimization tools still require a reasonable number of samples and iterations to explore the space efficiently. Further, it does not directly support template design, which is typically done by experts.

Second, we integrate the optimizer with expert input. Instead of using the optimizer for the inner loop and the expert for the outer loop, we combine them in both scenarios. For the inner loop, instead of evaluating the samples suggested by the optimizer, we query a larger number of samples and have an expert prune them. Further, we use the optimizer results to help experts explore new template designs. Our key insight is that the suggested samples can help users understand whether they are exploring the correct part of the design space and use this feedback to iterate on the template design.

By combining a design tool's search suggestions with human intuition about the knowledge of the mechanism and parameters that matter, we can expedite our optimization process and search of the design space as described below.

### *C. Design Iterations*

We create four design templates in Fig 5. Variations between templates include structural and geometric differences, as well as the number and ranges of design parameters. We used AutoOED [33, 34] for multi-objective Bayesian optimization to minimize weight and maximizing damping ratio. We explored templates that reduced the flybar's flexure stiffness to improve motion transfer between the flybar and the main rotor. We describe each template below.

*Template 1:* A rectangular design with a single connecting rod attached at a 90° angle between the flybar and main rotor (phase angle). We identified 4 design parameters for template 1, as shown in Fig 5A. Upon evaluation we observed significant stiffness in the structure and poor damping performance. After expert review, we expanded the designs space to include different phase angles.

*Templates 2:* A rounded design that allows for varying the connecting rod attachment points, resulting in different phase angles. A rotor blade leading edge was implemented. After prototyping 5 different design variations, the feedback from the computational design tool helped us realize there

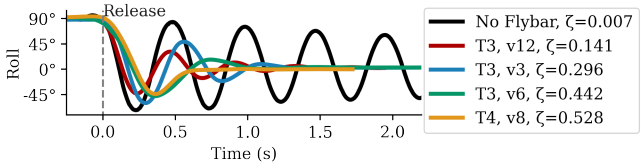


Fig. 6. **Prototype Template vs 1D Damping:** Roll angle response of flybar prototypes exhibiting different damping ratios when released from an angle of 90° on the 1D pendulum test fixture. Flybar designs with higher damping significantly reduce oscillation and improve stability.

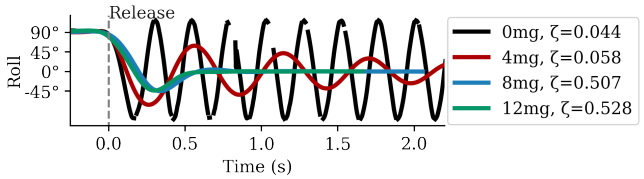


Fig. 7. **Counterweight vs 1D Damping:** Final Template flybar roll angle response with different counterweights show increased damping with increased counterweight. MoCap cameras occasionally miss data points.

were fundamental issues with the transferring of the motion of the upper flybar plate to the main rotor. We analyzed high-frame-rate video with an expert, concluding that the location of the connecting rod was increasing the system's stiffness.

*Template 3:* Fixed non-parallel axis of rotation between the flybar internal hinges, rotor internal hinges, and connecting rod hinges (see Fig 2B). We prototyped 3 design variations, enabling significant damping improvement. However, we were limited to phase angles of 90°, because non-90° phase angles resulted in flybar axis that did not rotate along the same axis as the rotor plate hinges, preventing feathering

*Final Template:* The final design allows for non-90° phase angles while maintaining the parallel axis of rotation for the flexures on the flybar and rotor plates in their local plane. A new connecting rod design (see Fig 5D) enabled 8 different flybar designs with simplified design parameters. Leveraging parameter values from Template 3 tests, we further optimized the damping ratio results characterized in the results section.

## IV. Results

### A. Test fixture

Our flybar aims to provide passive roll and pitch stability to a rotor. We built a custom test fixture for measuring damping effects in both 1D and 2D similar to those used to test prior insect scale robots [35]. The setup shown in Fig 8 consists of a circular platform suspended from two flexure joints which bend on the roll axis. The joints are produced using the method described in Fig 3 with FR4 substituted for carbon fiber. Orthogonal flexures for pitch motion are suspended from the circle and connect to a platform on which the motor is mounted. We create a 1D setup using glue to restrict the pitch hinges. The setup is attached to a wood frame with two 14 cm beams suspending the setup at 15 cm to reduce the ground effect. For 1D trials we attach an additional 144 mg balancing mass 20 mm below the motor.

### B. Damping Performance

We place the measurement setup from Fig 8 in a motion capture arena (4x Optitrack Prime 13, 240 fps) and attach

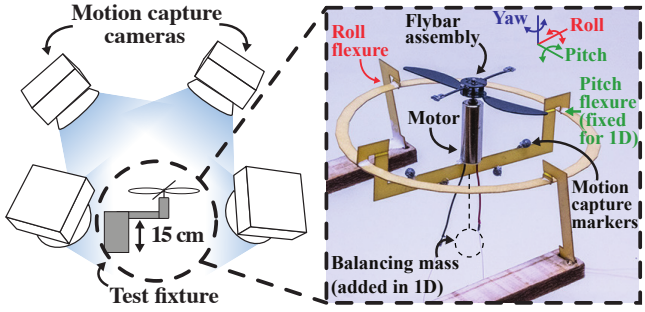


Fig. 8. Template 3 flybar mounted to a 2 axis test fixture restricting rotation to only pitch and roll. A 144 mg balancing mass is placed at the bottom of the 1 axis test setup to ensure that the system is at equilibrium when upright. Motion capture cameras are mounted around the test fixture.

four 1.5 mm retroreflective markers (B&L engineering) around the ring structure on our test fixture. For each design we perform three trials by tilting and releasing the motor from 90° to model a large angle disturbance. We simultaneously record videos of each experiment using a high frame rate camera (Phantom VR5.1, 5700 fps) Fig 6 shows the oscillation of the motor on the roll axis recorded by the motion capture cameras for a subset of 5 designs with varying damping ratios. Fig 7 shows the effect of counterweight on the damping ratio of Final Template prototypes. Increasing the counterweight mass from 0 mg to 12 mg improves the damping ratio, but increases stress on the connecting rods increases the likelihood of fracture and mechanical failure.

The motion can be approximated as a second order system: $\theta_{roll}(t) = e^{-\zeta\omega_n t}\cos(2\pi\omega_d t + \phi)$ where $\theta_{roll}$ is the rotation about the roll axis, $\zeta$ is the damping ratio, $\omega_n$ is the natural frequency of the system, $\omega_d$ is the damped natural frequency, and $\phi$ is the initial phase offset. We observe the structure consistently over or undershoots the target $\theta_{roll}$ of 0 indicating an underdamped response. We calculate the damping ratio of the system with the log decrement method [36] using the first two peaks of the signal. Considering the goal of our flybar is to produce damping and improve stability, we take this value as a figure of merit to compare designs.

Fig 6 shows that upon being released from a 90° angle, a rotor with no flybar is highly unstable and oscillates continuously with minimal damping. Through our series of design iterations we produce improving damping ratios up to a maximum of $\zeta = 0.528$. The higher values produce less oscillation and lower period of oscillation as expected and quickly settle to the steady state of 0. For example, at the highest damping ratio even after a large disturbance the system swings past 0 once undershooting the target but then reaches the steady state with minimal oscillation. The results highlight the effectiveness of the flybar in providing damping as well as the success of our iterative design process which improved $\zeta$ by 18.9x.

We compare our best performing design to a rotor with no flybar in a 2D test fixture using a high framerate camera and motion capture. Fig 9A shows the no flybar case where the rotor oscillates wildly. Our flybar in the same fixture shown in Fig 9B quickly stabilizes to steady state with a small angle bias of 8.5° due to slight assymetry in attachment and weight

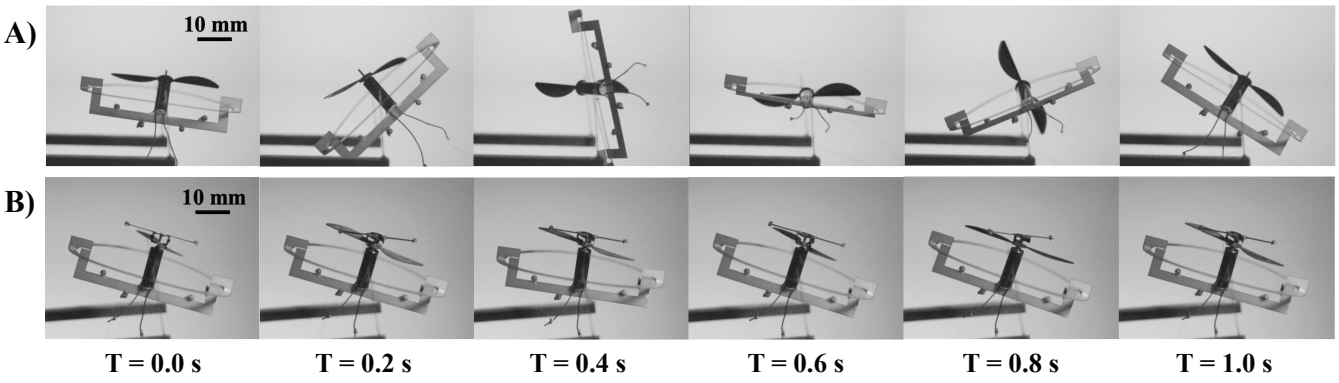


Fig. 9. A) Video frames from 1 s of a 2D stability test with no flybar showing a motor with near zero damping. B) Video frames from 1 s of a 2D stability test with our Final Template flybar achieving a damping ratio of ($\zeta = 0.528$). Small amounts of gyroscopic precession are seen about the center axis.

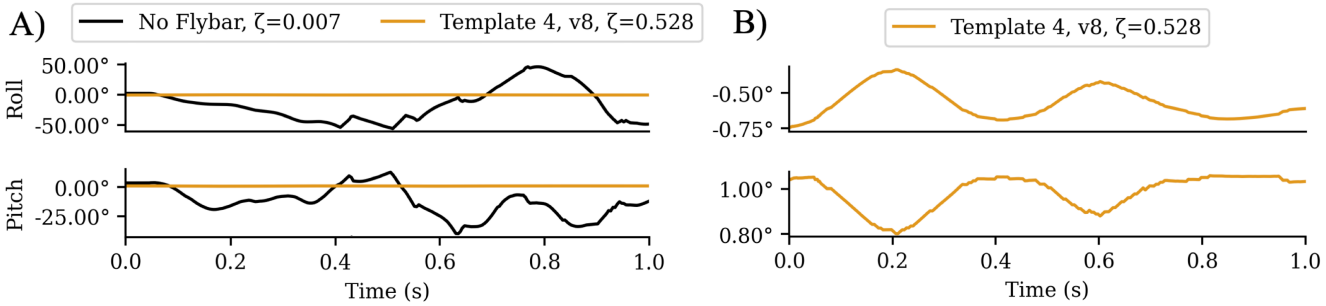


Fig. 10. Motion capture data from the same 2D test shown above. A) Pitch and roll angle response comparison of a flybar Final Template prototype and a rotor without a flybar. B) Zoomed-in pitch and roll angle response of a flybar Final Template prototype.

distribution on the test fixture. Motion capture data in Fig 9A confirms the chaotic $25 - 50°$ oscillations without the flybar compared to a small amount of gyroscopic precession about the center axis shown by a $< 0.5°$ oscillation in Fig 10B. Our results show, when combined with a counter-torque mechanism such as a tail rotor (which could be significantly smaller) to counteract this precession, our flybar will provide attitude stability for a millimeter scale helicopter.

## V. Discussion and Conclusion

We present a first of its kind flybar that can help stabilize a 2-3 cm rotor. We also present a novel workflow to design and optimize new small scale mechanisms by incorporating expert feedback into the design loop to explore the search space. At this scale, our flybar allows devices to leverage the high thrust of small motors while minimizing size, weight and power. Quadrotors require four motors for control, but with a single flybar stabilized rotor and a small tail rotor we could create a controlled helicopter at the 2-3 cm scale. This approach has the potential to allow for controlled flight whilst carrying a small onboard battery. Our flybar does not require active control, saving computation for other tasks. With the ability to generate 2.8 g of thrust with a ∼30 mm rotor, we can lift significant payload. This enables integrating an avionics system [3], battery [37], and sensors like cameras [38] bringing us a step closer to the longstanding vision of a fully autonomous sub-gram helicopter.

This work also opens up directions for future research. Helicopter controls are highly complex, and will require control algorithms compatible with the limited computation on small microcontrollers. Future works should also focus on additional modeling of the flybar dynamics. Integrating these models into the computational design workflow could more rapidly characterize the design space. Using expert feedback could also help prioritize useful regions of the design space.

## Acknowledgment

This research was supported by the National Science Foundation (award number FRR-2054850, GRFP award), the GEM Consortium Fellowship, a SPEEA ACE Fellowship, the Washington NASA Space Grant Consortium Fellowship, and the University of Washington's Herbold Fellowship.

## References

[1] N. Elkunchwar, S. Chandrasekaran, V. Iyer, and S. B. Fuller, "Toward battery-free flight: Duty cycled recharging of small drones," in *2021 IEEE/RSJ International Conference on Intelligent Robots and Systems (IROS)*. IEEE, pp. 5234–5241.

[2] Y. M. Chukewad, A. T. Singh, J. M. James, and S. B. Fuller, "A new robot fly design that is easier to fabricate and capable of flight and ground locomotion," *2018 IEEE/RSJ International Conference on Intelligent Robots and Systems (IROS)*, pp. 4875–4882, 2018.

[3] Y. P. Talwekar, A. Adie, V. Iyer, and S. B. Fuller, "Towards sensor autonomy in sub-gram flying insect robots: A lightweight and power-efficient avionics system," in *2022 International Conference on Robotics and Automation (ICRA)*. IEEE, 2022, pp. 9675–9681.

[4] Y. Chen, H. Zhao, J. Mao, P. Chirarattananon, E. F. Helbling, N.-s. P. Hyun, D. R. Clarke, and R. J. Wood,

"Controlled flight of a microrobot powered by soft artificial muscles," *Nature*, vol. 575, pp. 324–329, 2019.
[5] N. T. Jafferis, E. F. Helbling, M. Karpelson, and R. J. Wood, "Untethered flight of an insect-sized flapping-wing microscale aerial vehicle," *Nature*, 2019.
[6] M. Piccoli and M. Yim, "Piccolissimo: The smallest micro aerial vehicle," in *2017 IEEE International Conference on Robotics and Automation (ICRA)*. IEEE, 2017, pp. 3328–3333.
[7] "Cheerson cx10 mini drone." [Online]. Available: https://rcdrone.top/products/cheerson-cx10-mini-drone
[8] "Crazyflie2.1." [Online]. Available: https://www.bitcraze.io/products/crazyflie-2-1/
[9] T. Ozaki, N. Ohta, T. Jimbo, and K. Hamaguchi, "A wireless radiofrequency-powered insect-scale flapping-wing aerial vehicle," *Nature Electronics*, pp. 845–852, 2021.
[10] H. V. Phan and H. C. Park, "Mechanisms of collision recovery in flying beetles and flapping-wing robots," *Science*, vol. 370, no. 6521, pp. 1214–1219, 2020.
[11] F. Fei, Z. Tu, J. Zhang, and X. Deng, "Learning extreme hummingbird maneuvers on flapping wing robots," in *2019 International Conference on Robotics and Automation (ICRA)*. IEEE, 2019, pp. 109–115.
[12] S. Deng, M. Percin, and B. van Oudheusden, "Aerodynamic characterization of 'delfly micro'in forward flight configuration by force measurements and flow field visualization," *Procedia Engineering*, pp. 925–929, 2015.
[13] R. J. Wood, "The first takeoff of a biologically inspired at-scale robotic insect," *IEEE transactions on robotics*, vol. 24, no. 2, pp. 341–347, 2008.
[14] G. C. H. E. de Croon, K. M. E. de Clercq, R. Ruijsink, B. Remes, and C. de Wagter, "Design, aerodynamics, and vision-based control of the delfly," *International Journal of Micro Air Vehicles*, vol. 1, pp. 71–97, 2009.
[15] R. St. Pierre and S. Bergbreiter, "Toward autonomy in sub-gram terrestrial robots," *Annual Review of Control, Robotics, and Autonomous Systems*, pp. 231–252, 2019.
[16] "Motor brushed 4mm x 12mm, 7ohm," 2017. [Online]. Available: https://micronwings.com/product/motor-brushed-4mm-x-12mm-7-ohm-pack-of-3/
[17] W. S. Trimmer, "Microrobots and micromechanical systems," *Sensors and actuators*.
[18] K. Ma, P. Chirarattananon, S. B. Fuller, and R. J. Wood, "Controlled flight of a biologically inspired, insect-scale robot," *Science*, vol. 340, no. 6132, pp. 603–607, 2013.
[19] J. James, V. Iyer, Y. Chukewad, S. Gollakota, and S. B. Fuller, "Liftoff of a 190 mg laser-powered aerial vehicle: The lightest wireless robot to fly," *IEEE ICRA*.
[20] Y. M. Chukewad and S. Fuller, "Yaw control of a hovering flapping-wing aerial vehicle with a passive wing hinge," *IEEE Robotics and Automation Letters*, vol. 6, no. 2, pp. 1864–1871, 2021.
[21] G. J. Leishman, *Principles of helicopter aerodynamics with CD extra*. Cambridge university press, 2006.
[22] S. K. Kim and D. M. Tilbury, "Mathematical modeling and experimental identification of an unmanned helicopter robot with flybar dynamics," *Journal of robotic systems*, vol. 21, no. 3, pp. 95–116, 2004.
[23] S. Bai, Q. He, and P. Chirarattananon, "A bioinspired revolving-wing drone with passive attitude stability and efficient hovering flight," *Science Robotics*, vol. 7, no. 66, p. eabg5913, 2022.
[24] M. Piccoli and M. Yim, "Passive stability of vehicles without angular momentum including quadrotors and ornithopters," in *ICRA*. IEEE, 2015, pp. 1716–1721.
[25] ——, "Passive stability of a single actuator micro aerial vehicle," in *ICRA*. IEEE, 2014, pp. 5510–5515.
[26] S. B. Fuller, M. Karpelson, A. Censi, K. Y. Ma, and R. J. Wood, "Controlling free flight of a robotic fly using an onboard vision sensor inspired by insect ocelli," *Journal of The Royal Society Interface*, vol. 11.
[27] T. Uebori and K. Nakamura, "Rotor head of remotely-controlled helicopter and remotely-controlled helicopter," 2010, US Patent 20100196161A1.
[28] K. Jayaram, J. Shum, S. Castellanos, E. F. Helbling, and R. J. Wood, "Scaling down an insect-size microrobot, hamr-vi into hamr-jr," in *2020 IEEE International Conference on Robotics and Automation (ICRA)*. IEEE, 2020, pp. 10 305–10 311.
[29] Y. Koyama, I. Sato, D. Sakamoto, and T. Igarashi, "Sequential line search for efficient visual design optimization by crowds," *ACM Transactions on Graphics (TOG)*, vol. 36, no. 4, pp. 1–11, 2017.
[30] A. Zhao, J. Xu, M. Konaković-Luković, J. Hughes, A. Spielberg, D. Rus, and W. Matusik, "Robogrammar: graph grammar for terrain-optimized robot design," *ACM Transactions on Graphics*, pp. 1–16, 2020.
[31] H. Zhao, M. Willsey, A. Zhu, C. Nandi, Z. Tatlock, J. Solomon, and A. Schulz, "Co-optimization of design and fabrication plans for carpentry," *arXiv preprint arXiv:2107.12265*, 2021.
[32] M. Konakovic Lukovic, Y. Tian, and W. Matusik, "Diversity-guided multi-objective bayesian optimization with batch evaluations," *Advances in Neural Information Processing Systems*.
[33] Y. Tian, M. K. Luković, T. Erps, M. Foshey, and W. Matusik, "Autooed: Automated optimal experiment design platform," *arXiv preprint arXiv:2104.05959*, 2021.
[34] T. Erps, M. Foshey, M. K. Luković, W. Shou, H. H. Goetzke, H. Dietsch, K. Stoll, B. von Vacano, and W. Matusik, "Accelerated discovery of 3d printing materials using data-driven multiobjective optimization," *Science advances*, vol. 7, no. 42, p. eabf7435, 2021.
[35] D. Dhingra, Y. M. Chukewad, and S. B. Fuller, "A device for rapid, automated trimming of insect-sized flying robots," *IEEE Robotics and Automation Letters*, vol. 5, no. 2, pp. 1373–1380, 2020.
[36] D. J. Inman, "Engineering vibration," 2008.
[37] "Ultra low weight lithium ion batteries," https://www.powerstream.com/ultra-light.htm, PowerStream Technology, Tech. Rep., September 2013.
[38] V. Iyer, A. Najafi, J. James, S. Fuller, and S. Gollakota,

"Wireless steerable vision for live insects and insect-scale robots," *Science Robotics*, 2020.